International Journal of Thermal Sciences 112 (2017) 439–449

Contents lists available at ScienceDirect

International Journal of Thermal Sciences

journal homepage: www.elsevier.com/locate/ijts

Validity of the macroscopic energy equation model for laminar flows through porous media: Developing and fully developed regions

Federico E. Teruel [a, b, c, *]

[a] Centro Atómico Bariloche, CNEA, Bariloche 8400, Rio Negro, Argentina
[b] CONICET, Argentina
[c] Instituto Balseiro-Universidad Nacional de Cuyo, Argentina

ARTICLE INFO

Article history:
Received 23 March 2016
Received in revised form
7 November 2016
Accepted 7 November 2016
Available online 15 November 2016

Keywords:
Porous media
Macroscopic energy equation
Cellular average
Volume average
Developing region
Fully developed region

ABSTRACT

The performance of the macroscopic energy equation model for laminar flows through porous media is tested and analyzed in this study. This is achieved by comparing the behavior of the model with data obtained from microscopic numerical simulations. These simulations correspond to a flow that is heated by a constant temperature boundary condition at the fluid-solid interface in a simple porous structure formed by staggered square cylinders. Specifically, laminar steady flow regimes with $Re_D = 1$, 10 and 75, Pe_D in the 10-10^4 range, and porosities between 55 and 95% are simulated. Applying the cellular average to the numerical solution allows obtaining the macroscopic temperature. Results clearly show the existence of two different regions at a macroscopic scale. At the entrance, there is a thermally developing region characterized by a rapid variation of the temperature with the streamwise coordinate. The second region is the fully developed region where the non-dimensional temperature varies exponentially with the streamwise coordinate. The length of the developing region is found to be relatively large for high Pe_D numbers allowing to conclude that the thermal entrance effect cannot be neglected in the use of macroscopic models for large Pe_D numbers. The model is also tested in the fully developed region showing excellent agreement with the data. It is found that the decay rate of the macroscopic temperature in this region scales with $Pe_D^{-0.8}$ and that the exponent is fairly independent of the porosity, flow conditions and fluid properties. Finally, it is shown that models that ignore the entrance region or neglect thermal dispersion are, in general, not valid.

1. Introduction

Porous structures, such as fibrous porous media, spatially periodic solid structures and open cell foams are commonly found in many engineering and industrial applications such as grain storage, transport in soils, flow diffusers, cryogenic tanks, core of nuclear reactors, radiators, and so on. In many of these applications and under laminar [1–3] or turbulent flow conditions [4–8], porous structures are placed to interchange heat efficiently. In this study, the focus is on the modeling of the heat transfer process in porous structures under laminar flow conditions [1–3]. Findings of the present study can be applied to the modeling of a variety of devices as for example compact heat exchangers, electronic components, cooling towers, packed bed reactors and power transformers. Additionally, results of this study can be applied to the modeling of heat transfer at micro and nanoscale (e.g. Ref. [9]).

The goal of porous media models is to satisfactorily represent the macroscopic scale of a physical process without representing explicitly the physics at the microscopic scale (i.e. the scale of the pore [10–12]). The volume-averaging technique, employed as a space averaging tool, has been successful in the derivation of porous media models from conservation laws at a microscopic scale [13]. In particular, the macroscopic energy equation (or a macroscopic transport equation for a passive scalar) was originally derived in Refs. [14,15] and variations of its original form are commonly found in the literature (e.g. Refs. [4,16,17]). There are two main coefficients regarding the heat transfer phenomenon at a macroscopic scale: the interfacial heat transfer coefficient and the thermal dispersion tensor [10]. During the last four decades, much effort was devoted to measure these parameters experimentally for different flow conditions, different fluids, and different geometries (e.g. Ref. [18]). Nowadays, extensive research is carried out to

* Centro Atómico Bariloche, CNEA, Bariloche 8400, Rio Negro, Argentina.
E-mail address: teruel@cab.cnea.gov.ar.

http://dx.doi.org/10.1016/j.ijthermalsci.2016.11.005
1290-0729/

Nomenclature

a_{sf}	interfacial area per unit volume
C_p	fluid specific heat
h_{sf}	interfacial or macroscopic heat transfer coefficient
k_f	fluid thermal conductivity
$k_{D\text{-}xx}$	dispersion coefficient in the streamwise direction
p	pore length scale
u	local streamwise velocity
x^*	streamwise non dimensional coordinate ($x/2H$)
D	square-edge length
H	REV's dimension (REV volume = $2H$ x H)
$L_{5\%}$	thermal entrance length
Nu_D	macroscopic Nusselt number ($h_{sf}\,D/k_f$)
Pr	Prandtl number
Pe	Péclet number
Pe_D	Péclet number based on the Darcy velocity and D
Re	Reynolds number
Re_D	Reynolds number based on the Darcy velocity and D
T_B	bulk temperature
T_i	inlet fluid temperature
T_w	wall temperature
$\overline{T}$	intrinsic (fluid) cellular average of temperature
TEL	thermal entrance length
$\overline{U}$	intrinsic (fluid) cellular average of streamwise velocity
U_D	Darcy velocity ($\overline{U}\phi$)
V	volume of the REV
V_f	fluid volume inside the REV

Greek symbols

α	decay rate of macroscopic temperature
α_2	decay rate of macroscopic temperature neglecting diffusion effects
ϕ	porosity
ν	kinematic fluid viscosity
θ_{m}	microscopic non dimensional temperature
θ	macroscopic (intrinsic cellular average) non dimensional temperature
ρ	fluid density
ξ	local coordinate

Additional notations

$\overline{\psi}^{VA}$	volume average of φ
$\overline{\psi}^{CA}$	cellular average of φ
$\overline{\psi}$	intrinsic (fluid) cellular average of φ
${}^{i}\psi$	space fluctuation of φ
ΔL_{FD}	length difference between data and the fully developed model
$\%\Delta T_{FD}$	percentage temperature difference between data and the fully developed model

numerically compute these coefficients for different flow conditions, geometries, and fluid properties [19–21]. In general, these coefficients complete the macroscopic differential model for the transport of the macroscopic temperature.

As in the case of heat transfer in clear flows, the thermal entrance length (TEL) in a porous medium appears to be a relevant parameter to obtain. It is known, however, that the hydrodynamics entrance length in porous media, well discussed in Ref. [10], is of the size of a pore and therefore irrelevant at a macroscopic scale. Literature related to the TEL in porous media is scarce. Nevertheless, the experimental study of Wang and Du [22] provides some insight regarding this quantity. Measurements for the non-dimensional interfacial heat transfer coefficient (Nu_D) showed that this quantity evolves with the streamwise coordinate from a maximum at the entrance to a fully developed value in a distance equal to several equivalent diameters of the channel (the same general behavior is shown in Ref. [23]). In Ref. [24], Wang et al. analyzed further their data to find values for the TEL between 5 and 20 widths of the test section depending on the fluid properties and Reynolds number. Their results also showed that for the same flow conditions, the TEL is larger for the fluid with higher Prandt number. Wang et al. [24] also analyzed the data of [25] and [26] to calculate the TEL for two different experiments with air flowing through a porous medium. In this case, the TEL is between 2 and 4 widths of the test section. The numerical study of Imani et al. [27] also showed the dependence of the macroscopic heat transfer coefficient with the streamwise coordinate and the studies carried out by Teruel [23,29] and Teruel and Díaz [28] show the existence of a developing region that becomes larger when the Péclet number increases. Additionally, the experimental study of Han et al. [30] shows that the dispersivity in packed beds is a function of the streamwise position and that a developing length can be calculated measuring the spatial variation of this quantity. All the experimental evidence reviewed shows that the TEL is a macroscopic phenomenon that needs to be analyzed to find out its dependence on the characteristics of the porous medium, fluid properties and flow conditions.

Studies in the field also show that the use of the macroscopic energy equation is in general accompanied with some model assumptions. The most common assumption is to neglect the entrance effect in the thermal field. To neglect the streamwise thermal dispersion is also another findable assumption. For instance, in Refs. [31,32], analytical solutions of the macroscopic energy equation model are sought assuming constant values for the thermal dispersion and the interfacial heat transfer coefficients (i.e. the entrance effect is not considered). Another example of the use of such assumptions is the numerical study of Alfiere et al. [33]. The authors of this study are aware of the entrance effect but they acknowledged that to the best of their knowledge there is not an equation to calculate such effect in porous media flows. Regarding the assumption that neglects the streamwise thermal dispersion, this is done in Ref. [31] invoking a sufficiently high Péclet number or a highly convective flow. The study of Sano et al. [34] claimed an important statement on this regard: this coefficient, the thermal dispersion, may never be negligibly small for highly convective flows.

The main objective of this study is to test the validity of the macroscopic energy equation model in the laminar regime by comparing the solution of the macroscopic model with data obtained from microscopic numerical solutions in a porous structure. In particular, the study looks forward to give some insight over important aspects of the heat transfer process in laminar flows through porous media that, in the author's opinion, has been heretofore overlooked. One of them is the entrance effect in the thermal field. Another is the validity of the macroscopic energy equation model in the fully developed region. And finally, the assumption that the streamwise thermal dispersion can be neglected for high Péclet numbers flows. The work is organized as

follows. First, the macroscopic energy equation is presented and the main coefficients are defined; i.e., the macroscopic (or interfacial) heat transfer coefficient and the streamwise dispersion coefficient. The domain employed in the simulations is shown and a short description of the microscopic results is given. The space evolution of the macroscopic temperature is computed for all cases simulated. These results clearly show the existence of a developing region. The dependence of this region on fluid properties, flow conditions and geometry is then analyzed and the TEL is defined and computed. Later, the macroscopic model is tested against numerical data in the fully developed region. Finally, two usual approximations found in the literature are evaluated by comparing the model results with numerical data. The first approximation is based on a fully developed model that neglects the entrance effect and the second one is based on the use of a fully developed model that neglects dispersion effects.

2. Macroscopic energy equation via cellular average

Space averaging tools are often employed to develop macroscopic equations in porous media [10]. Consider a porous medium and an averaging volume (Representative Elementary Volume, REV) with centroid in the position $\underline{x}$ and radius $\underline{r}_0$. For averaging purposes, an auxiliary coordinate system $\underline{r} = \underline{x} + \underline{\xi}$ is defined, so that $\underline{x}$ describes the origin of each averaging volume and $\underline{\xi}$ is the position in a local coordinate system specific to each averaging volume. Take this volume as a constant (i. e. no space dependence) equals to the sum of the fluid and solid volumes inside the REV ($V = V_f(\underline{x}) + V_s(\underline{x})$). Following the formalism of [35,36], the Volume Average (VA) can be defined employing the weighting function $\boldsymbol{m_V}$:

$$m_v = \begin{cases} 1/V & if \quad |\underline{x} - \underline{r}| \le \underline{r}_o \\ 0 & if \quad |\underline{x} - \underline{r}| > \underline{r}_o \end{cases} \tag{1}$$

And a volume averaged quantity, $\overline{\psi}^{VA}$, is then calculated employing the convolution product * as:

$$\overline{\psi}^{VA}(\underline{x}) = m_v^* \left(\gamma_f \psi\right) = \int_{R^3} m_v(\underline{x} - \underline{r}) \gamma_f \psi(\underline{r}) dV_r, \tag{2}$$

where $\gamma_f(\underline{r})$ is a distribution function that takes the value one in the fluid phase and zero in the solid phase,

$$\gamma_f(\underline{r}) = \begin{cases} 1 & if \quad \underline{r} \in V_f \\ 0 & if \quad \underline{r} \in V_s \end{cases}. \tag{3}$$

Although the VA is frequently used in the literature to develop macroscopic equations [4–7,15–17], it has been shown that this averaging tool yields pore-scale fluctuations when employed in ordered media [23,28,35,36]. To solve this issue, Quintard and Whitaker [35,36] recommended the use of the Cellular Average (CA) for period structures. The CA is defined as in Equation (2) but employing a weighting function $\boldsymbol{m_C}$ defined as $\boldsymbol{m_C} = \boldsymbol{m_g}\,^* \boldsymbol{m_V}\,^* \boldsymbol{m_V}$. Mathematically, $\boldsymbol{m_C}$ is the double application of the volume average weighting function. The function $\boldsymbol{m_g}$ is introduced to satisfy the condition $m_C \in C^\infty$. It removes the discontinuity of the volume average weighting function at the boundary but does not modify, for continuous functions, the value of the macroscopic variable respect to the double application of the VA. For practical purposes and considering a REV with centroid at position $\underline{x}$, the CA of a fluid quantity ψ can be computed as:

$$\overline{\psi}^{CA}(\underline{x}) = \frac{1}{V} \int_V \overline{\psi}^{VA}(\underline{x} + \underline{\xi}) dV_\xi. \tag{4}$$

where $\overline{\psi}^{VA}$ can be computed as:

$$\overline{\psi}^{VA}(\underline{x}) = \frac{1}{V} \int_V \psi(\underline{x} + \underline{\xi}) \gamma_f dV_\xi, \tag{5}$$

Additionally, the space-decomposition of Hassanizadeh and Gray [37] can be used to decompose ψ in its intrinsic CA value (i.e. $\overline{\psi}(\underline{x}) = \overline{\psi}^{CA}(\underline{x})/\phi$) plus a local fluctuation in space as:

$$\psi(\underline{x} + \underline{\xi}) = \overline{\psi}(\underline{x}) + {}^i\psi(\underline{x} + \underline{\xi}). \tag{6}$$

Applying Equations (3)–(6) and the generalization of the averaging theorem [36] to the microscopic equations (i.e. energy and momentum conservation in the fluid), a macroscopic set of equations can be obtained. For an isothermal fluid that enters to a constant porosity porous medium with constant wall temperature, the macroscopic momentum equations simple reduce to a constant CA velocity in the streamwise direction. However, the macroscopic energy equation must be capable to accurately describe the behavior of the CA temperature when the fluid flows and transfers heat in the porous medium. Under considerations of steady, incompressible, one-dimensional flow (x-direction) in a constant porosity medium with constant wall temperature, the transport equation for the macroscopic fluid temperature resumes (see Ref. [4] for the same equation but based on volume average quantities):

$$\rho C_p \phi \overline{U} \frac{d\overline{T}}{dx} = \frac{d}{dx}\left[\phi\left(k_f + k_{D-xx}\right)\frac{d\overline{T}}{dx}\right] + h_{sf} a_{sf} \left(T_w - \overline{T}\right). \tag{7}$$

Which is a convection-diffusion equation with the intrinsic CA temperature, $\overline{T}$, as dependent variable. This equation is characterized by two macroscopic coefficients, the interfacial heat transfer (h_{sf}) and the streamwise thermal dispersion ($k_{D\text{-}xx}$). These two coefficients are generally defined from modeling assumptions and conservation criteria. The interfacial heat transfer, or its equivalent non dimensional number, Nu_D, is defined to assure the conservation of energy:

$$Nu_D = \frac{h_{sf} D}{k_f} = \frac{D}{k_f} \frac{\frac{1}{V}\int_V \left[\frac{1}{V}\int_{A_{sf}} k_f \nabla T \cdot d\vec{A}\right] dV}{a_{sf}\left(T_w - \overline{T}\right)}. \tag{8}$$

and the streamwise thermal dispersion is defined employing a diffusion hypothesis [10] following the ideas of Taylor [38] and Aris [39]:

$$k_{D-xx} = -\rho C_p \frac{\frac{1}{V_f}\int_V \left[\frac{1}{V}\int_V {}^i u\, {}^i T\, dV\right] dV}{\nabla_x \overline{T}}. \tag{9}$$

These two macroscopic parameters were studied in detail in the flow configuration under consideration in Ref. [23] for the same set of simulations analyzed in this study. Computed fully developed values for Nu_D and $k_{D\text{-}xx}$ were in excellent agreement with data available in open literature. Values in the developing region were also qualitatively well compared with available experimental data. In the present study, the focus is on the macroscopic energy

Equation (7) as a model to successfully represent the macroscopic temperature in laminar flows through porous media.

3. Numerical method and domain of study

A schematic diagram of the domain selected for the simulation is shown in Fig. 1. The fluid flows from left to right, entering the porous medium after flowing a distance of H as a clear flow. The porous medium extends in the streamwise direction from $x = 0$ to a location between $x = 48H$ and $x = 220H$, depending on the flow conditions. Therefore, the porous region has between 24 and 110 REVs in a row (the REV is chosen as a cell of $2H$xH in the streamwise and spanwise directions respectively). As it will be understood later, this large domain is chosen so that the flow achieves fully developed conditions for high Péclet numbers. The fluid-solid interface is set to a different temperature than that in the fluid at the entrance. But this is done at the location $x = 6H$ to achieve a smooth transition in the CA temperature in the entrance region and to allow the flow to develop hydrodynamically. To save computational time, only the bottom half of the REV ($H/2$) is simulated. This simplification is based on the fact that simulations of a single REV with periodic BCs evolve to steady solutions at the Reynolds numbers simulated in this study [40,41].

The governing equations for the fluid phase (mass, momentum and energy respectively) are given as follows:

$$\nabla\cdot\underline{u} = 0, \tag{10}$$

$$\frac{\partial \underline{u}}{\partial t} + (\nabla \underline{u})\cdot\underline{u} = -\nabla p + \frac{1}{\mathrm{Re}}\nabla^2\underline{u}, \tag{11}$$

$$\frac{\partial T}{\partial t} + \nabla\cdot(\underline{u}T) = \frac{1}{Pe}\nabla^2 T. \tag{12}$$

Boundary conditions are standard for all the boundaries of the domain, except at the outlet, where periodic BCs are applied. On the solid walls BCs resume:

$$\underline{u} = \underline{0},\ T = \left\{ \begin{array}{ll} T_i & x < 6H \\ T_w & x \geq 6H \end{array} \right\}. \tag{13}$$

On the inlet of the domain (uniform field):

$$\underline{u} = (p/H, 0),\ T = T_i. \tag{14}$$

On the bottom and top horizontal lines of the domain (symmetry):

$$\nabla_n \underline{u} = \underline{0}, \nabla_n T = 0. \tag{15}$$

And on the outlet of the domain (periodicity):

$$\underline{u}(x_o, y) = \underline{u}(x_o - 2\mathrm{H}, y), \tag{16}$$

$$T(x_o, y) = T_w + \tau(T(x_o - 2\mathrm{H}, y) - T_w), \tag{17}$$

where x_o indicates the x-coordinate of the outlet; and τ is defined as:

$$\tau = \frac{T_B(x) - T_w}{T_B(x - 2H) - T_w}, \tag{18}$$

where T_B is the bulk temperature of the fluid. Equation (17), the periodicity for temperature, has been discussed in detail by Teruel and Díaz [28] and others [19].

To solve the set of Equations (10)–(12) under BCs given in Equations (13)–(17), the SIMPLER algorithm developed by Patankar [42] was employed. The diffusion and the convective terms were modeled with central differences and the QUICK scheme respectively [43,44]. To evolve the initial condition to the steady state a backward Euler scheme was used. The solver has been fully tested and validated for different geometries, including those presented in this study [40,41]. Periodic variables were solved in an iterative manner, and profiles at the outlet were obtained from previous time steps according to Equations (16) and (17). Simulations were considered to reach convergence when normalized residuals were lower than 10^{-6}. It has been carefully checked that numerical solutions conserve energy in a global sense (domain) and in local sense (REV).

The domain was discretized using a uniform and structured grid of squares, and a systematic grid refinement study was carried out. Macroscopic quantities reported in this study were found to be independent of any further grid refinement for the calculation of macroscopic variables. The grid resolution employed for each REV was 180 × 45 ($2H$ x $H/2$, streamwise x vertical direction), 128 × 32 and 180 × 45 for 55, 75 and 95% porosity respectively. The porosity is defined as $\phi = 1 - D^2/H^2$ according to Fig. 1.

The Reynolds number based on the Darcy velocity and size of the obstacles, Re_D, was varied from 1 to 75. As it was mentioned, three different porosities were simulated 55, 75 and 95%. The Pe_D number, defined as $Re_D\,Pr$, was varied from 50 to 10^4 for the cases of 55 and 75% porosity, and between 10 and 5000 for 95% porosity. Data of a total of seventy-eight simulations is presented.

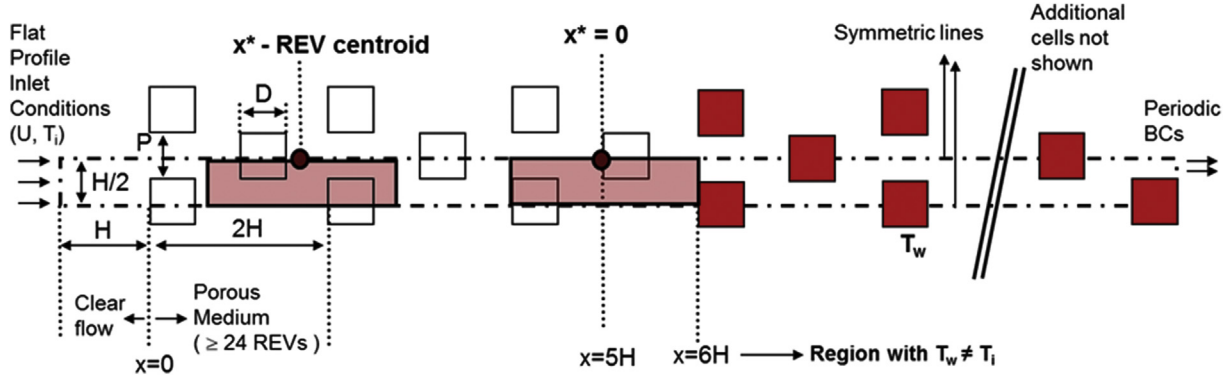

Fig. 1. Geometry of the domain simulated (smallest domain 49H x $H/2$, largest domain 221H x $H/2$). Case of a free stream entering the porous medium.

4. Results and discussion

4.1. Behavior of the macroscopic temperature: developing and fully developed regions

In order to better understand the CA temperature it is useful to analyze the microscopic solution for the temperature in the porous structure by representing contours of the spatial evolution of non-dimensional microscopic temperature, $\theta_m(x^*) = (T(x^*) - T_w)/(T_i - T_w)$. Fig. 2 shows that the higher the porosity the slower the temperature variations with the streamwise coordinate. This effect is not only due to the variation of the interfacial area with porosity but also due to the sinuous path that the flow follows in the porous structure. This is reflected at the macroscopic scale as a decrease of Nu_D and an increase of $k_{D\text{-}xx}$ increasing the porosity [23].

With the numerical data at hand (Fig. 2), the CA temperature can be computed in the entire domain employing a moving REV in the streamwise direction and a discrete equivalent of Equation (4). Note that the CA temperature is only dependent on the horizontal coordinate due to the periodicity in the vertical direction. Fig. 3 shows the spatial evolution of macroscopic non-dimensional temperature $\theta_m(x^*) = (\overline{T}(x^*) - T_w)/(T_i - T_w)$. In particular, part a) of this figure shows this evolution for 55% porosity and $Re_D = 1$, and part b) for 95% porosity and $Re_D = 75$. Fig. 3 shows two interesting aspects to consider. First, the reason to employ such a large domain in the streamwise direction is revealed. For large Pe_D numbers the temperature evolves slowly to its equilibrium value (i.e. in more than a couple of REVs). This is even true for the 55% porosity case, for which it is expected that the CA temperature evolves faster than at higher porosities. For the case of 95% porosity and $Pe_D = 5000$, the value of θ reduces from 1 to 0.6 in 100 REVs in a row (note that in Fig. 2 only 12 REVs in a row are shown). And second, the large set of values simulated for Pe_D yields a large variation in the decay rate of θ allowing to test the macroscopic energy equation model under a large variety of conditions.

To easily understand the behavior of the CA temperature shown in Fig. 3, it is useful to recall the case of a channel flow with constant wall temperature. For this well studied case, after a developing region, there is a fully developed (FD) region characterized by an exponential behavior of the non-dimensional bulk temperature. Although Fig. 3 shows an apparent exponential decay of the macroscopic temperature with the streamwise coordinate, a closer look at the entrance region reveals the existence of a developing and a FD region. Fig. 4 shows in linear-log scale some particular cases of those shown in Fig. 3. A straight line that fits the macroscopic temperature far away from the inlet is superimposed to each curve to show the deviation of the data from a model based on an exponential decay. A fully developed region is qualitative indicated in Fig. 4 for the curve with higher Pe_D considering a position where the exponential decay deviates a given percentage from the data.

A FD model can be easily obtained by analytically solving the macroscopic energy Equation (7) under the assumption that macroscopic coefficients are constants (i.e. non space dependent). The model then yields the following analytical expression:

$$\theta(x^*) = \frac{\overline{T}(x^*) - T_w}{T_i - T_w} = e^{-\alpha x^*}. \tag{19}$$

where in Equation (19), the decay rate, α, is a function of the macroscopic parameters as well as the flow and medium properties:

$$\alpha = \frac{1 - \sqrt{1 + 4AC}}{2A}, \quad A = \frac{\sqrt{1-\phi}}{2}\frac{1}{Pe_D}\left(1 + \frac{k_{D-xx}}{k_f}\right), \quad C = \frac{8Nu_D}{Pe_D}\sqrt{1-\phi}. \tag{20}$$

Equation (19) will be called the FD model and is represented by a straight-line in a linear-log scale as those shown in Fig. 4. Therefore, if the FD model is valid, data obtained from numerical experiments should follow a straight-line in the proper scale. Note that this assumption, that neglects the entrance effect, is in general employed when macroscopic models are used [9,31,32,34,45] and it was clearly shown in Fig. 4 that the CA temperature develops to a fully developed state after a thermal entrance length (similar to the case of a channel flow with constant wall temperature as boundary condition). For large Pe_D numbers, Fig. 4 suggests that the region where the temperature does not obey the FD model can be relatively large making a FD model inadequate. As found in a previous study [23], the macroscopic interfacial coefficient and the streamwise thermal dispersion computed with Equations (8) and (9) respectively, are space dependent in the entrance region. Therefore, the macroscopic energy equation must be solved considering this fact to capture the right trend. If this fact is ignored, errors given by the model must be quantified to deal with model uncertainties. The next section is dedicated to study the aspects that allow quantifying these errors. The first aspect to consider is the TEL.

4.2. Developing region: the thermal entrance length

As pointed out in the experiment by Han et al. [30], the streamwise thermal dispersion is space-dependent in the entrance region. The experiment of Wand and Du [22] also shows that the macroscopic heat transfer coefficient is space-dependent in the entrance region. For the numerical experiment under consideration, Teruel [23] showed that both, the streamwise thermal dispersion and the macroscopic heat transfer coefficients show the entrance effect before reaching a FD constant value. Naturally, if an exponential model is assumed for the macroscopic temperature, α must be also space dependent to match the numerical data shown

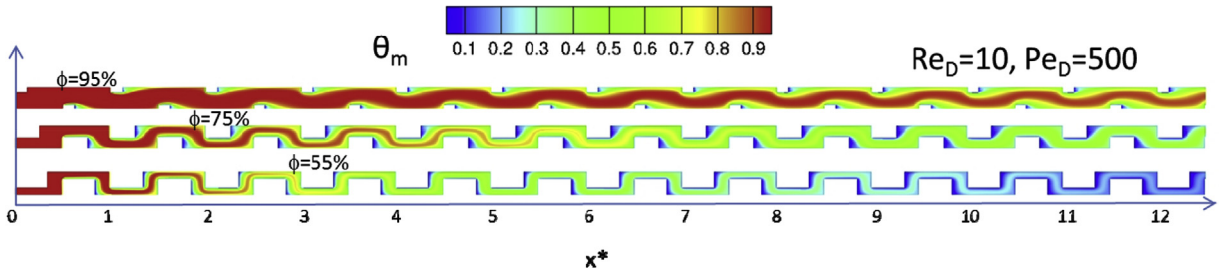

Fig. 2. Contours of θ_m for different porosities (55, 75 and 95%). $Re_D = 10$ and $Pe_D = 500$. Note that $x^* = x/2H$ and that the origin of this macroscopic coordinate is equal to $5H$ (Fig. 1).

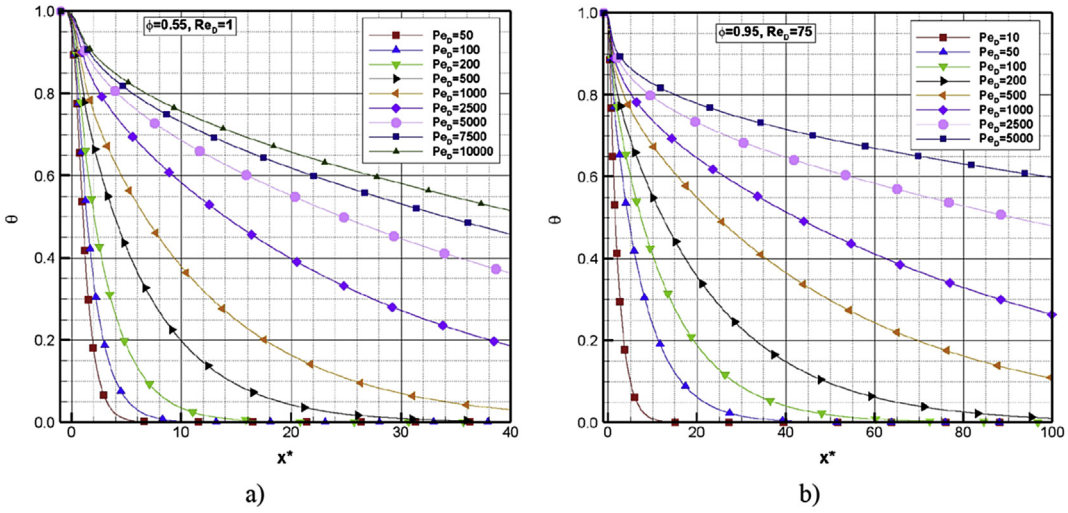

Fig. 3. Space evolution of θ. Pe_D as a parameter. a) 55% porosity, $Re_D = 1$. b) 95% porosity, $Re_D = 75$.

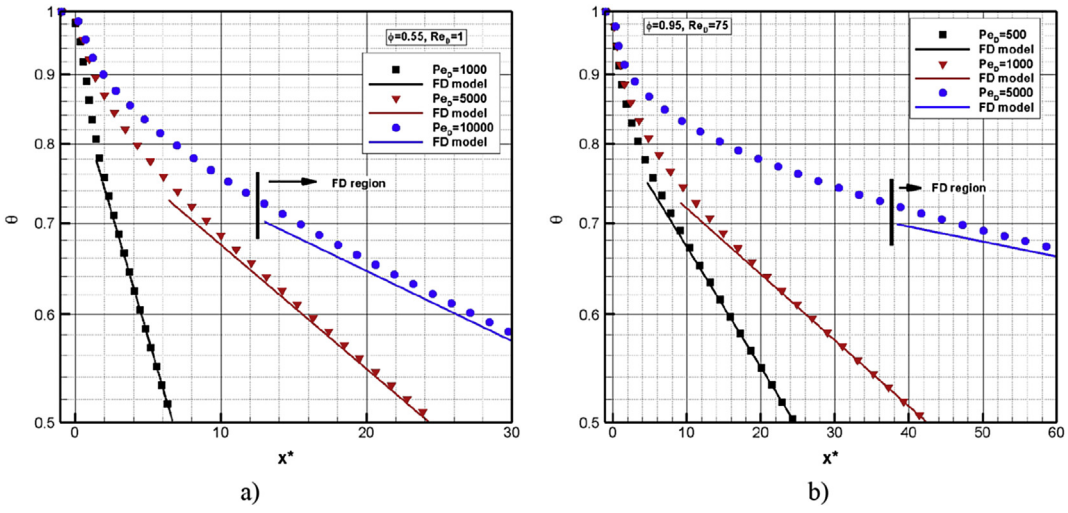

Fig. 4. Space evolution of θ. Differences respect to an exponential decay. a) 55% porosity, $Re_D = 1$. b) 95% porosity, $Re_D = 75$.

in Fig. 4. Fig. 5 shows the spatial evolution of these three relevant macroscopic coefficients, Nu_D, $k_{D\text{-}xx}$ and α, for two different Pe_D numbers. Note that Nu_D and $k_{D\text{-}xx}$ are computed employing the discrete versions of Equations (8) and (9) respectively. The coefficient α is computed with Equation (20). This equation is strictly valid when Nu_D and $k_{D\text{-}xx}$ are constant but it is an excellent approximation when these coefficients are close to their FD values. For this reason the α-coefficient is plotted in Fig. 5 only for those locations where both, Nu_D and $k_{D\text{-}xx}$, are within a 20% difference of their FD values. The α-coefficient, calculated with Equation (20), shows a similar behavior than that found for Nu_D. However, the α-coefficient needs more distance than the heat transfer coefficient to reach a given difference respect to its FD value due to the slow variation of $k_{D\text{-}xx}$.

The thermal entrance length is an important parameter in the heat transfer process. It is used to define a location in the flow from where the behavior of the heat transfer process is known. That is, the heat transfer coefficient becomes approximately constant or the behavior of the temperature follows a known law. For instance, for the case of the channel flow with constant surface temperature, this parameter is usually defined as the distance where the heat transfer coefficient reaches a 5% difference respect to its FD value [46]. After this distance, the non-dimensional bulk temperature may be assumed to vary exponentially with the streamwise coordinate. For the case under consideration, and different from the channel flow case, in the developing region there are two macroscopic parameters that are space dependent, Nu_D and $k_{D\text{-}xx}$. Although any of them may be used to define the TEL, and in fact, they reach the FD region in approximately the same distance (see Fig. 5), it seems appropriate from a practical point of view to define the TEL as the location from where the non-dimensional CA temperature exhibits, approximately, an exponential variation with the streamwise coordinate. This behavior is controlled directly by α. Therefore, the α-coefficient is chosen in this study to define the TEL. This allows using the FD model downstream of the TEL with an error bar that can be easily estimated based on the percentage difference between the value of this coefficient respect to its FD value.

The thermal entrance length, $L^*_{5\%}$, is then defined as the non-dimensional location (x^*) from where the decay rate, $\alpha(x^*)$, computed with Equation (20), differs in less than 5% respect to its FD value. This criterion is exemplified in Fig. 5 for 75% porosity,

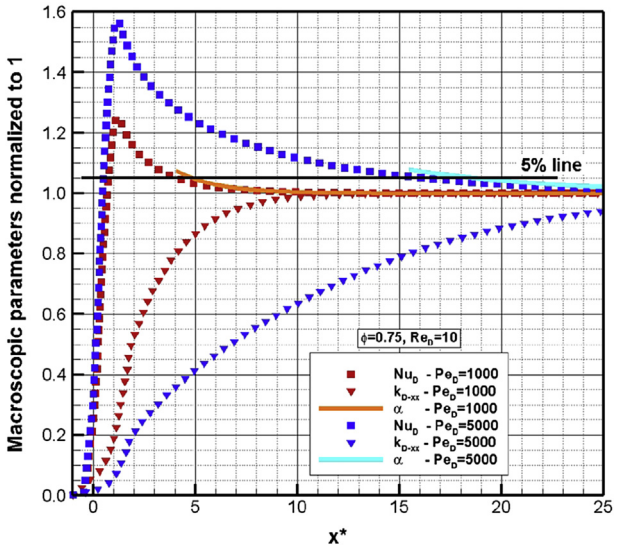

Fig. 5. Space evolution of macroscopic coefficients (Nu_D, $k_{D\text{-}xx}$ and α). Values are normalized with FD values. 75% porosity, $Re_D = 10$.

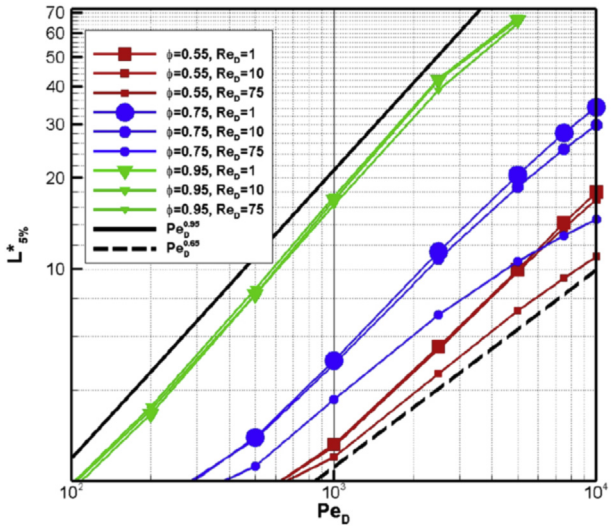

Fig. 6. Dependence of the TEL on Pe_D. Porosity and Re_D as parameters. Cases with $L^*_{5\%} > 2$.

$Re_D = 10$ and two different Pe_D numbers. In this figure, $L^*_{5\%}$ is defined as the location where the 5% line cuts the α-curve. Two important aspects need to be considered in the definition of $L^*_{5\%}$. The first one is that this quantity is determined based on numerical experiments and employing Equation (20). The second one is that it is assumed that the FD model is valid for locations greater that $L_{5\%}$. This assumption will be tested in the next section. It is also important to say that the behavior shown in Fig. 5 regarding the space evolution of the macroscopic coefficients was found to be the same for all cases simulated in this study with $Pe_D > 100$ [23]. Therefore, the definition chosen for $L^*_{5\%}$ assures that the difference in the macroscopic heat transfer coefficient respect to its FD values is below 5% for locations greater than $L^*_{5\%}$.

Values reported in Table 1 are also reported in Figs. 6–8 to have a clear understanding of the dependence of the TEL on the porosity, Re_D and Pe_D. Fig. 6 has been limited to data with $L^*_{5\%} > 2$ (or equivalently, large Pe_D), as for lower values there is not enough spatial resolution in the data to show a trend. Additionally, in Fig. 6, two particular lines have been added to show qualitatively the dependence of this quantity on Pe_D (note that in each line Re_D is keep constant and therefore only the Prandtl number is varying). For the data simulated, the TEL increases as fast as $Pe_D^{0.95}$ for 95% porosity and as low as $Pe_D^{0.65}$ for 55% porosity. The TEL is larger than 2 for Pe_D larger than 1000, larger than 500 and larger than 200 for 55%, 75% and 95% porosity respectively. The largest calculated $L^*_{5\%}$ is

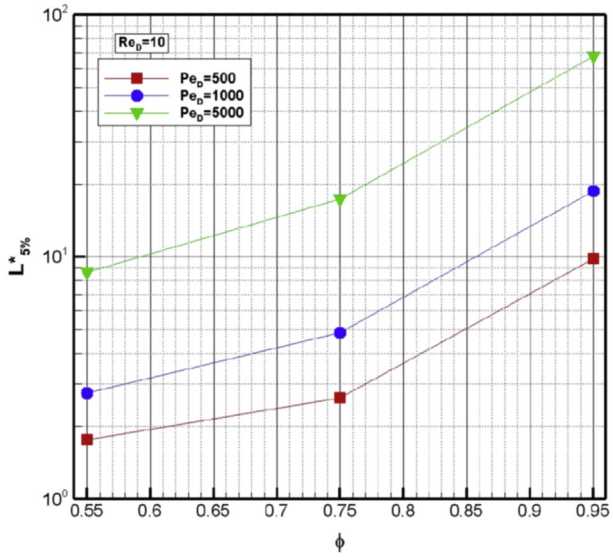

Fig. 7. Dependence of the TEL on the porosity. Pe_D as parameter and $Re_D = 10$.

equal to 67.5 REVs in a row for the case of 95% porosity, $Re_D = 10$ and $Pe_D = 5000$. Data clearly shows that the TEL can be significant

Table 1
Values for the TEL ($L^*_{5\%}$) for all cases simulated.

$L_{5\%}$									
Pe_D	$\phi = 55\%$			$\phi = 75\%$			$\phi = 95\%$		
	$Re_D = 1$	$Re_D = 10$	$Re_D = 75$	$Re_D = 1$	$Re_D = 10$	$Re_D = 75$	$Re_D = 1$	$Re_D = 10$	$Re_D = 75$
10							1.0	1.0	1.0
50	1.3	1.3	1.2	1.1	1.0	1.0	1.2	1.3	1.3
100	1.2	1.2	1.1	1.0	0.9	0.9	1.9	2.0	1.9
200	1.0	1.0	1.4	1.6	1.6	1.5	3.3	3.5	3.5
500	1.8	1.8	1.8	2.8	2.7	2.2	8.3	8.6	8.3
1000	2.6	2.6	2.4	5.0	4.9	3.7	16.9	17.4	16.3
2500	5.6	5.5	4.5	11.4	10.8	7.1	42.1	42.5	38.9
5000	10.0	9.8	7.3	20.5	18.7	10.6	66.3	67.5	64.4
7500	14.2	13.7	9.4	28.1	24.9	12.9			
10000	17.9	17.0	11.0	34.3	29.9	14.6			

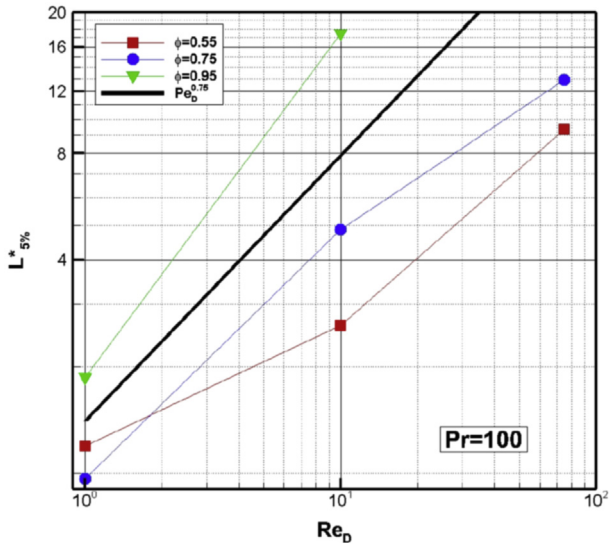

Fig. 8. Dependence of the TEL on Re_D. Porosity as parameter. $Pr = 100$.

in the length of the flow domain and that it increases rapidly with Pe_D for laminar flow conditions. This makes the applicability of the FD model questionable.

The dependence of the TEL on the porosity is shown in Fig. 7 (for constant Re_D and Pe_D). Data shows that this quantity increases approximately one order of magnitude varying the porosity from 0.55 to 0.95. The dependence of the TEL on the Re_D is now considered (i.e. considering the same fluid properties). With the set of parameters simulated it is only possible to show the case of $Pr = 100$. Fig. 8 shows that the strong dependence of this quantity on the Re_D can be roughly estimated as $L_{5\%} \propto \mathrm{Re}_D^{0.75}$.

Although this study does not provide enough data to develop a correlation for the TEL, a qualitative comparison can be done with the well-known channel flow case. For the circular tube with diameter D, the TEL for laminar flows can be correlated as $x/D = 0.55\, Re_D Pr$ [46]. For the porous medium under study it can be proposed $L_{5\%} \propto \mathrm{Re}_D{}^a \mathrm{Pr}^b$, where the exponents a and b are mainly functions of the porosity. By inspection of Fig. 6, it can be concluded that the exponent b varies between 0.65 and 0.95, and is weakly dependent on Re_D. By inspection of Fig. 8, the exponent a can be roughly approximated by the value of 0.65 for high Pr.

4.3. Fully developed region

4.3.1. Decay rate: model vs. numerical data

It has already been shown that from the macroscopic point of view there is a region where the flow is thermally developing. It is clear than in this region the FD model is not adequate (this will be quantified in the next section). In addition, the validity of the FD model in the FD region needs to be evaluated by testing the definitions adopted for the macroscopic coefficients (Equations (8) and (9)). This approach is rarely found in the literature (see exceptions in Refs. [33,34]) but it is essential as it shows the capability of the model to predict the correct evolution of the macroscopic temperature. Therefore, to test the validity of the model in the FD region, the decay rate is computed in two different ways. First, it is computed fitting the macroscopic temperature near the outlet in Fig. 1, specifically in the last four REVs. In this region the exponential decay is fully established as it is proved by a correlation coefficient for the fit higher than 0.999. And second, it is computed according to Equation (20), employing values calculated for the macroscopic coefficients in the FD region [23]. These two values are then compared. Table 2 shows the decay rate obtained from the fitted values and the percentage difference between the α obtained from the data and that obtained from the model (Equation (20)) to the value obtained from the data. Differences are below 2% for all cases simulated except for two particular cases (discussed below). Therefore, the agreement between the fitted data and the model is excellent for the large variety of parameters simulated (note that α varies two orders of magnitude with the range of Pe_D simulated). It is then concluded that the convection-diffusion model with the definitions given for the macroscopic parameters employing the CA tool is very accurate for the FD region. The two exceptions where the model does not fit the data are i) the CA temperature develops in a relatively short distance (approximately a couple of REVs) and there is not enough spatial resolution to compute the decay rate accurately (the lowest Pe_D simulated and 55% porosity) and ii) the developing region is even larger than the domain simulated and therefore, the macroscopic parameters cannot be calculated with high precision (the largest Pe_D simulated and 95% porosity). Note that this implies that values presented in Table 1 for this last case are not very accurate.

Other aspect of interest is the dependence of the decay rate as a function of the Pe_D number. This is shown in Fig. 9, where the fitted decay rate is shown for all cases simulated. This global parameter can be well approximated by $\alpha \propto Pe_D{}^{-0.8}$. The exponent seems to be fairly independent of ϕ and Re_D for cases simulated in this study.

4.3.2. Approximation employing the fully developed model

Calculations of energy transfer employing porous media models are commonly found in the literature. It has been shown in the previous section that these types of models are very accurate in the FD region. However, it is frequently assumed that fully developed conditions are applicable to the entire domain [9,30,31,33,34,45]. Moreover, in some cases, dispersion affects are also neglected

Table 2
Decay rate in the FD region. Values obtained from numerical data and percentage difference with respect to values obtained with the model.

	$Re_D = 1$		$Re_D = 10$		$Re_D = 75$	
	α-fitted	% difference	α-fitted	% difference	α-fitted	% difference
a) 55% porosity						
50	1.0750	4.6	1.0808	4.3	1.1468	4.5
100	0.6094	1.5	0.6130	1.4	0.6677	1.5
200	0.3359	0.3	0.3372	0.5	0.3798	0.5
500	0.1526	0.1	0.1536	0.1	0.1779	0.2
1000	0.0840	0.1	0.0847	0.1	0.1003	0.1
2500	0.0380	0.0	0.0385	0.0	0.0475	0.0
5000	0.0210	−0.1	0.0214	0.0	0.0277	0.0
7500	0.0149	−0.1	0.0154	0.0	0.0205	0.0
10000	0.0118	0.0	0.0123	0.0	0.0167	0.0
b) 75% porosity						
50	0.4747	1.0	0.4898	1.0	0.5225	1.1
100	0.2625	0.3	0.2715	0.3	0.3068	0.4
200	0.1460	0.1	0.1510	0.1	0.1793	0.2
500	0.0673	0.0	0.0699	0.0	0.0886	0.1
1000	0.0373	0.0	0.0391	0.0	0.0517	0.0
2500	0.0171	0.0	0.0182	0.0	0.0255	0.0
5000	0.00973	−0.1	0.0105	0.0	0.0152	0.0
7500	0.00711	−0.3	0.00772	−0.1	0.0115	0.0
10000	0.00585	−0.1	0.00628	0.0	0.00942	0.0
c) 95% porosity						
10	0.4103	0.7	0.4574	0.8	0.4765	0.9
50	0.1097	0.1	0.1232	0.1	0.1349	0.1
100	0.0625	0.0	0.0695	0.1	0.0773	0.0
200	0.0356	0.0	0.0392	0.0	0.0432	0.0
500	0.0168	0.0	0.0184	0.0	0.0203	0.0
1000	0.00944	0.0	0.0103	0.0	0.0111	0.0
2500	0.00438	−0.4	0.00470	−0.3	0.00486	−0.2
5000	0.00250	−2.6	0.00263	−2.9	0.00253	−5.1

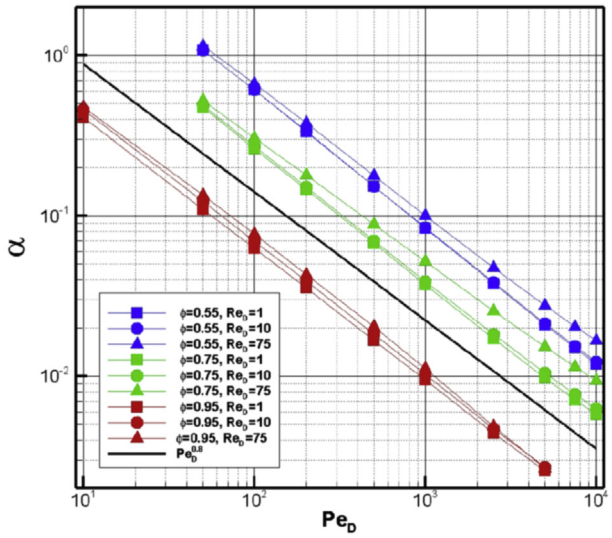

Fig. 9. Fitted decay rate as a function of Pe_D. Porosity and Re_D as parameters.

[9,30,45]. See the discussion of Sano et al. [34] and Yang and Nakayama [47] in these regards. Although these assumptions might be valid for some flow conditions, they have not been clearly identified. As it will be shown in this study, these assumptions yield large errors in the calculation of the temperature field and are not recommended for porous media flows such as those analyzed in this study. This is now discussed in detail comparing numerical values of the CA temperature with those obtained by models based on these assumptions. First, it is considered a hypothetical case where the decay rate is measured experimentally in the fully developed region (i.e. α is known experimentally). Fig. 10 shows the actual temperature for a particular case simulated in this study and the temperature obtained from a FD model characterized by the measured decay rate. It is illustrative to consider two situations to evaluate differences that may appear if this model is employed. First and considering the CA temperature, the percentage difference between the data and the model to the value of the data is calculated ($\%\Delta T_{FD}$). And second, the length difference to achieve a given temperature between the data and the model (ΔL_{FD}) is also calculated. Note that these two quantities are independent on the space coordinate in the FD region.

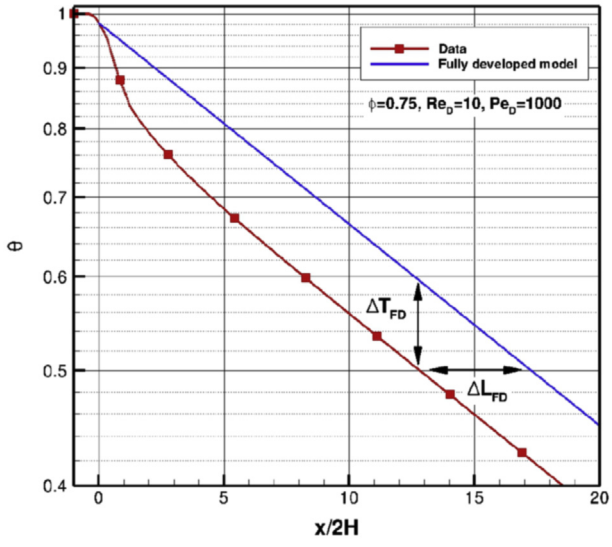

Fig. 10. Space evolution of the CA temperature. Numerical data and a FD model that matches the inlet condition.

These two parameters are given in Table 3 for cases where the TEL is larger than 2. The parameter $\%\Delta T_{FD}$ ranges from −5% to −41% and it increases, as expected, with Pe_D and Re_D. If for example the length of a heat exchanger is fixed, the outlet temperature calculated with the FD model will be between 5 and 41% higher than the real value. The values of ΔL_{FD} range between −1 and −50. These parameters also increase with Pe_D and Re_D. If for example a heat exchanger is designed to achieve a given outlet temperature, the length of the heat exchanger calculated with the FD model will be overestimated between 1 and 50 REVs in a row for the parameters simulated in this study. These analyses show that the FD model should be employed with great care in the laminar regime and it is not applicable for large Pe_D numbers if the TEL is not considered.

4.3.3. Approximations employing the FD model and neglecting the dispersion coefficient

Now, the other assumption that is employed in the literature is evaluated: models that neglect dispersion effects. The analytical solution of this type of models is:

$$\theta(x^*) = \frac{\overline{T(x^*)} - T_w}{T_i - T_w} = e^{-\alpha_2 x^*}, \tag{21}$$

where the new decay rate (α_2) is calculated neglecting the diffusion term:

$$\alpha_2 = -C,\ C = \frac{8Nu_D}{Pe_D}\sqrt{1-\phi}. \tag{22}$$

This assumption is based on the fact that the streamwise thermal dispersion is much larger that the thermal diffusion [23] and that the first one is negligibly small respect to the source term in Equation (7) or respect to the convective term in the case of large Péclet numbers [33,47]. For the cases simulated in this study, it will be shown that the α_2-coefficient is a poor approximation of α, meaning that even, in the FD region, this model is not adequate. Table 4 shows calculated values of α_2 for all the cases simulated and the percentage difference with respect to the value of α. The percentage differences are between 10 and 40% in the majority of the cases simulated. These differences decrease with the porosity and

Table 3
$\%\Delta T_{FD}$ and ΔL_{FD} for all cases simulated.

	$\%\Delta T_{FD}$			ΔL_{FD} (x^*)		
	$Re_D = 1$	$Re_D = 10$	$Re_D = 75$	$Re_D = 1$	$Re_D = 10$	$Re_D = 75$
a) 55% porosity						
1000	−12.0	−16.0	−28.0	−1.3	−1.8	−2.5
2500	−16.0	−18.5	−35.0	−4.0	−4.5	−6.3
5000	−18.0	−20.5	−39.0	−8.0	−8.8	−12.0
7500	−19.0	−21.5	−40.0	−11.8	−12.5	−16.5
10000	−19.8	−22.0	−41.0	−15.0	−16.0	−20.5
b) 75% porosity						
500	−11.0	−16.0	−25.0	−1.5	−2.0	−2.5
1000	−14.0	−19.0	−30.0	−3.5	−4.5	−5.0
2500	−16.5	−22.0	−35.8	−8.8	−11.0	−12.0
5000	−18.0	−23.3	−36.0	−17.0	−20.0	−20.0
7500	−18.8	−23.5	−35.8	−23.5	−27.0	−26.5
10000	−19.0	−23.5	−35.0	−29.0	−33.0	−32.0
c) 95% porosity						
200	−5.5	−9.0	−14.8	−1.5	−2.0	−3.0
500	−7.5	−11.5	−19.8	−4.0	−5.8	−9.0
1000	−8.7	−13.3	−23.3	−9.0	−12.0	−19.0
2500	−11.0	−16.0	−27.0	−21.0	−31.0	−50.0

Table 4
Calculated values for α_2 and its percentage difference respect to α.

	$Re_D = 1$		$Re_D = 10$		$Re_D = 75$	
	α_2	% difference	α_2	% difference	α_2	% difference
a) 55% porosity						
50	1.2609	−17	1.3051	−16	1.5036	25
100	0.7051	−16	0.7305	−17	0.8738	29
200	0.3852	−15	0.3985	−18	0.4959	30
500	0.1743	−14	0.1802	−17	0.2338	31
1000	0.0959	−14	0.0992	−17	0.1331	33
2500	0.0434	−14	0.0451	−17	0.0642	35
5000	0.0240	−14	0.0251	−17	0.0378	37
7500	0.0172	−14	0.0181	−17	0.0281	37
10000	0.0136	−15	0.0144	−17	0.0230	38
b) 75% porosity						
50	0.5436	−15	0.5858	−20	0.6701	−28
100	0.2984	−14	0.3225	−19	0.3922	−28
200	0.1653	−13	0.1789	−18	0.2306	−29
500	0.0761	−13	0.0828	−18	0.1161	−31
1000	0.0422	−13	0.0464	−19	0.0690	−33
2500	0.0195	−14	0.0217	−19	0.0345	−35
5000	0.0111	−14	0.0125	−20	0.0207	−36
7500	0.0081	−14	0.0092	−19	0.0155	−35
10000	0.0066	−14	0.0075	−20	0.0126	−34
c) 95% porosity						
10	0.4438	−8	0.5057	−11	0.5272	−11
50	0.1167	−6	0.1351	−10	0.1513	−12
100	0.0663	−6	0.0763	−10	0.0879	−14
200	0.0377	−6	0.0430	−10	0.0508	−18
500	0.0178	−6	0.0202	−10	0.0241	−19
1000	0.0100	−6	0.0114	−11	0.0134	−21
2500	0.0047	−6	0.0052	−11	0.0060	−23
5000	0.0026	−2	0.0029	−6	0.0032	−19

increase with Re_D. This implies that the temperature predicted by the model rapidly deviates from the data.

It is also important to note that although in the clear flow case the streamwise diffusion term is negligible in the limit of large Péclet numbers, for the macroscopic model and laminar flows it is not. Specifically, if Equation (7) is rescaled so that the coefficient of the convective term is 1, the coefficient of the diffusion term is then rescaled according to Equation (20):

$$A = \frac{\sqrt{1-\phi}}{2}\frac{1}{Pe_D}\left(1+\frac{k_{D-xx}}{k_f}\right). \tag{23}$$

And knowing that $k_{D-xx}/k_f \propto Pe_D^2$ (see for example [23]), it is concluded that this term cannot be neglected in the limit of high Pe_D because $A \propto Pe_D$ while the coefficient of the convective term is 1.

5. Concluding remarks

The performance of the macroscopic energy equation model for laminar flows through porous media has been studied and analyzed. For that purpose, a large set of numerical simulations were carried out. These simulations allowed to obtain the space evolution of the macroscopic temperature in a simple porous medium by averaging microscopic numerical results. The domain was large enough to allow simulations of laminar flow with large Péclet numbers ($Pe_D = 10^4$).

As in the well known case of the heat transfer in a channel, the macroscopic temperature exhibits two regions regarding the heat transfer process: a developing region and a fully developed region. In the first region, the macroscopic temperature does not obey the exponential law. The length of the developing region was defined as the location where the decay rate of the non-dimensional temperature (α), calculated with the FD model, is within 5% of its FD value. With this definition, it is found that the TEL is relatively large for large Pe_D numbers. In particular, the TEL is larger than 2 REVs in a row for Pe_D larger than 1000, 500 and 200 for 55, 75 and 95% porosity respectively. Additionally, the TEL can be as large as 10, 20 and 66 REVs in a row for the same porosities and $Pe_D = 5000$. This quantity was shown to increase with the Prandt number and Re_D but at a lower rate than that found in the clear channel flow case. It also increases approximately an order of magnitude changing the porosity from 55% to 95% for fixed Re_D and Pe_D. These results allow to conclude that the thermal entrance effect cannot be neglected for large Pe_D numbers.

Data in the fully developed region is characterized by an exponential decay of the non-dimensional temperature. In this region, the fully developed model has an analytical solution characterized by a decay rate dependant on the macroscopic parameters, geometry and flow conditions. This decay rate was calculated based on numerical data and computed based on model assumptions. The agreement between both quantities was excellent proving that the fully developed model can accurately describe the fully developed region. Moreover, it was found that the decay rate scales with $Pe_D^{-0.8}$ and that the exponent is fairly independent on the porosity, flow conditions and fluid properties for the large range of parameters simulated in this study.

Another important aspect considered in this study was the evaluation of two assumptions that are often made when homogeneous models are employed. One of them is the assumption of the fully developed conditions from the entrance. It was proved that for laminar flows and especially for large Pe_D numbers, this assumption is not valid. If this assumption is made, it was found that in the FD region there is a significant percentage different between the numerical temperature and that obtained from the model ($\%\Delta T_{FD}$), or there is a significant difference between the lengths needed to achieve a given temperature (ΔL_{FD}) calculated with the data and with the model. The other assumption often made in the literature is to neglect streamwise dispersion effects. The decay rate was then calculated based on this assumption. These values were substantially different from those computed from the data. Moreover, it was shown that for laminar flows, dispersion effects cannot be neglected even in the limit of large Pe numbers because the streamwise dispersion coefficient increases as Pe_D^2.

The results of this study indicate that for devices that employ liquid metals or gases as working fluids ($Pr < 1$) it is valid to neglect the TEL at macroscopic scale (the Pe_D number is lower than 75 in the steady laminar regime). However, for working fluids such as water or freon ($1 < Pr < 50$), depending on the porosity and Re_D number, the TEL will be measurable but bounded by approximately 5 REVs. Also, for working fluids with high Pr numbers such as engine oils or some alcohols ($Pr > 100$), the FD model is not applicable and the TEL will drastically extend for distances larger than those computed in this study. One application that exemplified the last case is the power transformers that employ dielectric oil as a cooling fluid.

Acknowledgements

This work was supported by grants from Universidad Nacional de Cuyo (PB 2013–2015), from ANPCyT-FONCyT (PICT 2012-2575) and from CONICET (PIP 112 201301-00829 CO).

References

[1] Vijay D, Goetze P, Wulf R, Gross U. Forced convection through open cell foams based on homogenization approach: transient analysis. Int J Therm Sci 2015;98:1–14.
[2] Takemoto Y, Kawanishi K, Mizushima J. Heat transfer in the flow through a bundle of tubes and transitions of the flow. Int J Heat Mass Transf 2010;53:5411–9.

[3] Pathak MG, Ghiaasiaan SM. Convective heat transfer and thermal dispersion during laminar pulsating flow in porous media. Int J Therm Sci 2011;50:440–8.
[4] Nakayama A, Kuwahara F, Kodama Y. An equation for thermal dispersion flux transport and its mathematical modelling for heat and fluid flow in a porous medium. J Fluid Mech 2006;563:81–96.
[5] Pinson F, Gregoire O, Quintard M, Prat M, Simonin O. Modeling of turbulent heat transfer and thermal dispersion for flows in flat plate heat exchangers. Int J Heat Mass Transf 2007;50:1500–15.
[6] Saito MB, de Lemos MSJ. A correlation for interfacial heat transfer coefficient for turbulent flow over and array of square rods. J Heat Transf 2006;128:444–52.
[7] Teruel FE, Rizwan-uddin. Numerical computation of macroscopic turbulence quantities in representative elementary volumes of the porous medium. Int J Heat Mass Transf 2010;53:5190–8.
[8] Nimvari ME, Maerefat M, El-Hossaini MK. Numerical simulation of turbulent flow and heat transfer in a channel partially filled with a porous media. Int J Therm Sci 2012;60:131–41.
[9] Buonomo B, Manca O, Lauriat G. Forced convection in micro-channels filled with porous media in local thermal non-equilibrium conditions. Int J Therm Sci 2014;77:206–22.
[10] Kaviany M. Principles of heat transfer in porous media. Springer-Verlag; 1991.
[11] Vafai K. Handbook of porous media. Taylor & Francis Group; 2005.
[12] Ingham DB, Pop I. Transport phenomena in porous media II. Elsevier Ltd.; 2005.
[13] Whitaker S. The method of volume averaging. Kluwer; 1999.
[14] Cheng P. Heat transfer in geothermal systems. Adv Heat Transf 1978;14:1–105.
[15] Carbonell RG, Whitaker S. Dispersion in pulsed systems-II. Theoretical developments for passive dispersion in porous media. Chem Eng Sci 1983;38:1795–802.
[16] Amaral Souto HP, Moyne C. Dispersion in two-dimensional periodic porous media. Part II. Dispersion tensor. Phys Fluids 1997;9:2253.
[17] Saada MA, Chikh S, Campo A. Analysis of hydrodynamics and thermal dispersion in porous media by means of a local approach. Heat Mass Transf 2006;42:995–1006.
[18] Wakao N, Kaguei S. Heat and mass transfer in packed beds. New York: Gorden and Breach; 1982. p. 243–95.
[19] Kuwahara F, Shirota M, Nakayama A. A numerical study of interfacial convective heat transfer coefficient in two-energy equation model for convection in porous media. Int J Heat Mass Transf 2001;44:1153–9.
[20] Gamrat G, Favre-Marinet M, Le Person S. Numerical study of heat transfer over banks of rods in small Reynolds number cross-flow. Int J Heat Mass Transf 2008;51:853–64.
[21] Pedras MHJ, de Lemos MJS. Thermal dispersion in porous media as a function of the solid–fluid conductivity ratio. Int J Heat Mass Transf 2008;51:5359–67.
[22] Wang BX, Du JH. Forced convective heat transfer in a vertical annulus filled with porous media. Int J Heat Mass Transf 1993;36:4207–13.
[23] Teruel FE. Entrance effect on the interfacial heat transfer and the thermal dispersion in laminar flows through porous media. Int J Therm Sci 2016;104:172–85.
[24] Wang BX, Du JH, Peng XF. Internal natural, forced and mixed convection in fluid-saturated porous medium, Transport phenomena in porous media. Pergamon; 1998.
[25] Coberly CA, Marshall Jr WR. Temperature gradients in gas streams flowing through fixed granular beds. Chem Eng Prog 1951;47:141–50.
[26] Yagi S, Kunni D. Studies of heat transfer near wall surface in packed beds. AIChE J 1960;6:97–104.
[27] Imani GR, Maerefat M, Hooman K. Estimation of heat flux bifurcation at the heated boundary of a porous medium using a pore-scale numerical simulation. Int J Therm Sci 2012;54:109–18.
[28] Teruel F, Díaz L. Calculation of the interfacial heat transfer coefficient in porous media employing numerical simulations. Int J Heat Mass Transf 2013;60:406–12.
[29] Teruel F. Calculation of the interfacial heat transfer and streamwise dispersion coefficients employing double volume average. In: Proc FEDSM2013, 1C; 2013. art. 16119.
[30] Han N, Bhakta J, Carbonell RG. Longitudinal and lateral dispersion in packed beds: effect of column length and particle size distribution. AIChE J 1985;31:277–88.
[31] Kuznetsov AV, Nield DA. Thermally developing forced convection in a porous medium occupied by a rarefied gas: parallel plate channel or circular tube with walls at constant heat flux. Transp Porous Media 2009;76:345–62.
[32] Ouyang XL, Vafai K, Jiang PX. Analysis of thermally developing flow in porous media under local thermal non-equilibrium conditions. Int J Heat Mass Transf 2013;67:768–75.
[33] Alfieri F, Tiwari MK, Zinovik I, Brunschwiler T, Michel B, Poulikakos D. On the significance of developing boundary layers in integrated water cooled 3D chip stacks. Int J Heat Mass Transf 2012;55:5222–32.
[34] Sano Y, Kuwahara F, Mobedi M, Nakayama A. Effects of thermal dispersion on heat transfer in cross-flow tubular heat exchangers. Heat Mass Transf 2011;48:183–9.
[35] Quintard M, Whitaker S. Transport in ordered and disordered porous media I: the cellular average and the use of weighting functions. Transp Porous Media 1994;14:163–77.
[36] Quintard M, Whitaker S. Transport in ordered and disordered porous media II: generalized volume averaging. Transp Porous Media 1994;14:179–206.
[37] Hassanizadeh M, Gray WG. General conservation equations for multi-phase systems: 1. Averaging procedure. Adv Water Resour 1979;2:131–44.
[38] Taylor GI. Dispersion of soluble matter in solvent flowing slowly through a tube. Proc Roy Soc A 1953;219:186–203.
[39] Aris R. On the dispersion of a solute in a fluid flowing through a tube. Proc Roy Soc A 1956;235:67–77.
[40] Díaz L. Desarrollo de una herramienta numérica para el cálculo de parámetros macroscópicos en medios porosos bidimensionales. Thesis for the degree of Mechanical Engineer. Argentina: Instituto Balseiro, Universidad Nacional de Cuyo; 2012.
[41] Teruel FE. Macroscopic turbulence modeling and simulation for flow through porous media. Ph.D. thesis. Urbana-Champaign, IL: University of Illinois; 2007.
[42] Patankar SV. Numerical heat transfer and fluid flow, hemisphere. 1980.
[43] Leonard BP. A stable and accurate convective modeling procedure based on quadratic upstream interpolation. Comput Methods Appl Mech Eng 1979;19:59–98.
[44] Hayase T, Humphrey JAC, Greif R. A Consistently formulated QUICK scheme for fast and stable convergence using finite-volume iterative calculation procedures. J Comput Phys 1982;98:108.
[45] Cheng L, Kuznetsov AV. Heat transfer in a laminar flow in a helical pipe filled with a fluid saturated porous medium. Int J Therm Sci 2005;44:787–98.
[46] Incropera FP, DeWitt DP. Fundamentals of heat and mass transfer. Springer-Verlag; 1991.
[47] Yang C, Nakayama A. A synthesis of tortuosity and dispersion in effective thermal conductivity of porous media. Int J Heat Mass Transf 2010;53:3222–30.